Hindawi
Advances in Civil Engineering
Volume 2022, Article ID 3787756, 12 pages
https://doi.org/10.1155/2022/3787756

Research Article

Dynamic Property Analysis of Orthotropic Bridge Deck with Local Fatigue Crack

Zhao Li[1,2], **Jiarui Zhang**[1,2], **Yaoyang Zhu**[1,2] and **Jianwei Tu**[1,2]

[1]*State Key Laboratory of Silicate Materials for Architecture, Wuhan University of Technology, Wuhan 430070, China*
[2]*Hubei Key Laboratory of Roadway Bridge and Structure Engineering, Wuhan University of Technology, Wuhan 430070, China*

Correspondence should be addressed to Jiarui Zhang; zjr1207916099@whut.edu.cn and Jianwei Tu; tujianwei@whut.edu.cn

Received 10 December 2021; Accepted 8 March 2022; Published 8 April 2022

Academic Editor: Ayman Ahmed Seleemah

With the increase in traffic volume and overweight vehicles, fatigue problems are highlighted. Especially for the orthotropic steel deck, the premature cracks seriously affect the service performance, operation, and service quality of the bridge. In this paper, the steel box-girder segment model and deck substructure model considering several typical fatigue cracks were established to reveal the variation law of fatigue cracks on vibration frequency and deflection under vehicle traveling load. A natural frequency analysis was performed to evaluate the change in the vibration characteristics due to localized damage, together with a dynamic analysis that considered a vehicle traveling on the bridge. The results show that the initiation and propagation of several typical cracks have little influence on the lower modes of the overall structure and great influence on the high-order modes of the substructure. The dynamic deflection response of the bridge changed under vehicle load as damage progressed. Therefore, it was possible to identify cracks of the orthotropic steel bridge deck and to provide guidance for fatigue crack detection and repair.

1. Introduction

Orthotropic steel decks (OSDs) have been widely used in bridges with various structural forms and spans due to the advantages of lightweight, favorable mechanical behavior, and convenient construction [1–4], as well as for deck replacement in existing bridges [5, 6]. However, the welding defects and residual stress are easily introduced into the manufacture and construction because of the complex geometric structure forms and structural discontinuity, which may be quite susceptible to traffic-induced fatigue damage [7–10]. An increasing number of investigations indicate that the failures of most steel bridges are caused by fatigue damage [11, 12]. In addition, the crack of the Bronx-Whitestone bridge [13] after 2 years in service and the collapse of the I-35 W bridge over the Mississippi River [14] have aroused attention to the fatigue and fracture of the existing bridge. The emergence of fatigue cracks seriously affects the operation and durability and even endangers the safety of bridges.

The fatigue damage of OSD is still a prominent problem because the cyclic vehicle load directly acts on the deck, especially accidental overloaded trucks [15–17]. Another adverse effect concerning the fatigue behavior of OSD is that the local stress near the crack caused by residual stress and live load stress ranges is concentrated to a high level, which is generally considered to be the main cause of the fatigue and fracture under cyclic vehicle load [18–20]. The typical fatigue cracks of OSD generally observed are illustrated in Figure 1 [21–23]: (1) the longitudinal rib-to-diaphragm welded joint and the cutout of the diaphragm plate; (2) the longitudinal rib-to-deck welded joint; (3) the longitudinal ribs splice joint; (4) the deck-to-vertical stiffener welded joint. During the past decades of engineering practice, many improvements have been achieved, such as structural design and manufacture, crack monitoring, and maintenance. Obviously, the fatigue cracks at the deck-to-vertical stiffener welded joint have been gradually replaced due to the change of the welded joint. Nevertheless, since the first fatigue crack of OSD was reported, the fatigue problem has restricted the development of this type of bridge.

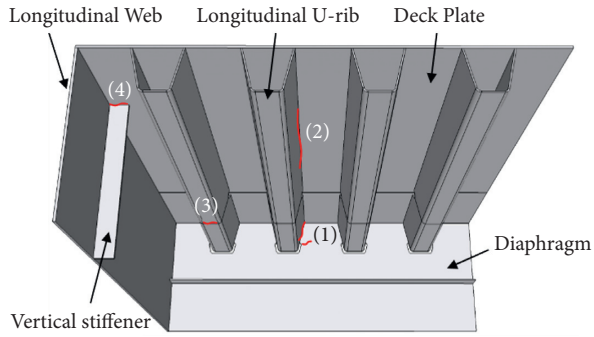

Figure 1: Sketch of typical fatigue cracks of OSD.

Many research studies on fatigue resistance have been devoted to the typical fatigue crack of OSDs in test and analysis. From the achieved research, the longitudinal rib-to-deck welded joint is the most common connection and the most sensitive position for fatigue in OSDs, due to direct wheel loading. A considerable amount of research has a focus on this topic [24–26]. Zhang et al. [27] established a local finite element model of OSDs to study the stress distribution of the deck in the longitudinal rib-to-deck welded joint and estimate the fatigue life using the principle of linear elastic fracture mechanics. The results indicate that the high-stress range under the local overloaded wheel is the main reason for the cracks in the longitudinal rib-to-deck welded joint. The principle of linear elastic fracture mechanics can be used to estimate the residual life of the longitudinal rib-to-deck welded joint. Kainuma et al. [28, 29] carried out the fatigue tests and FE analysis to study the structural response, local stress, and the mechanism of crack initiation and propagation near the longitudinal rib-to-deck welded joint. The results show that both the tensile stress and the stress range have an effect on crack initiation, but tensile stress is the important factor for crack propagation. In addition, the root gap shape and the penetration rate have an impact on fatigue durability. Sim et al. [30] investigated the effects of weld melt-through and distortion control measures on the fatigue behavior of the longitudinal rib-to-deck welded joint through six full-scale OSD fatigue tests. The results show that the effective precambering was beneficial to the fatigue resistance of the longitudinal rib-to-deck welded joint. Most cracks are initiated from the weld toe outside the rib. In the orthotropic steel deck, the longitudinal rib-to-diaphragm welded joint is another place prone to fatigue cracks [31]. The investigations of this weld detail indicated that the fatigue crack is mainly caused by the local stress at the weld root or toe generated by in-plane and out-of-plane bending moments [32]. In addition, the stress gradients were so notable that it was not feasible to evaluate fatigue resistance for this weld joint using the simple nominal stress approach. The proposal of notch stress and hot spot stress effectively solves the problem that it is very difficult to evaluate the fatigue assessment of the longitudinal rib-to-diaphragm welded joint [33–37]. The longitudinal rib is the main stress component of the orthotropic steel deck, which plays an extremely important role in increasing the stability and stiffness of the bridge. However, longitudinal rib splice joints generally adopt overhead welding with incomplete penetration and undercut. The crack is most likely to initiate at the stress concentration point and even propagate to a larger size [38, 39]. A related study on the fatigue resistance of the longitudinal rib splice joints indicated that the fatigue cracks are mainly observed at the transverse weld of longitudinal rib bottom plate because of incomplete penetration.

The above research results of typical fatigue cracks with different details effectively improve the fatigue resistance and deepen the understanding of the fatigue damage mechanism of OSD. However, with the increasing traffic volume and accidental overload, fatigue cracks still seriously affect the durability of bridges. In order to explore the influence of several typical fatigue cracks on the mechanical properties of OSD, the steel box-girder segment model and deck substructure model are established. And, a natural frequency analysis was performed to evaluate the change in the vibration characteristics due to localized damage, together with a dynamic analysis that considered a vehicle traveling on the bridge. According to the research results of this paper, it is possible to predict the location of several typical fatigue cracks in the orthotropic steel deck and to provide a reference for crack maintenance.

2. Analysis Method

2.1. Main Analysis Contents. The natural frequency analysis and dynamic analysis were carried out using the finite element analysis software [40] Ansys15.0 with a steel box-girder segment model and a substructure model. The following were studied:

(1) Global vibration modes analysis for the steel box-girder segment model including crack damage at low frequency

(2) Local vibration modes analysis for the steel substructure model including crack damage at high frequency

(3) Dynamic analysis considering a vehicle traveling on the bridge

2.2. Finite Element Model. The steel box-girder model was based on the in-service cable-stayed bridge including 4 fast lanes and 2 slow lanes. The cable-stayed bridge has a total length of 684 m and a main span of 336 m. The steel deck support is composed of 4 concrete auxiliary piers, 2 concrete towers 106 m higher than the bridge deck, and 104 cables with different pretension. Relevant research shows that there is a high probability of cracks in the red U-rib area. More than 50% of fatigue cracks were located in the third lane, which is mainly used for low-speed truck driving, and few cracks were detected in the first lane [41]. The half cross-sectional view of the steel box girder of the bridge is shown in Figure 2. The 24 m segment model has 3 vertical suspenders on each side with a spacing of 12 m. The steel box girder has a width of 32.8 m and a depth of 3.2 m. The bridge is designed with a 16 mm orthotropic deck, 12 mm bottom plate, 8 mm

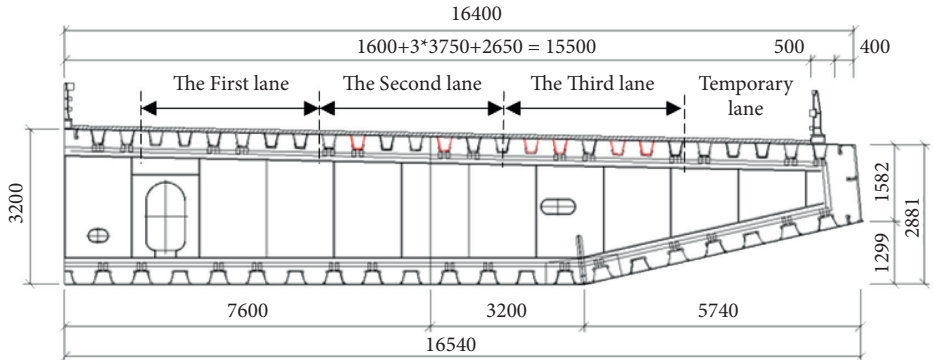

Figure 2: The half cross-sectional view of the steel box girder.

longitudinal U-ribs at the top, and 6 mm longitudinal U-ribs at the bottom. The longitudinal U-ribs are 280 mm high and placed at 600 mm centers. The width of the longitudinal U-ribs at the top and bottom are 300 and 400 mm, respectively. The orthotropic deck is supported on 10 mm transverse diaphragms every 3 m. In order to avoid stress concentration, the diaphragm under the longitudinal U-ribs is designed as an arc-shaped notch, and the details of the notch are shown in Figure 3.

The steel box-girder segment model and the substructure model of the orthotropic steel deck were established to accurately simulate the mechanical properties of a steel bridge. All plate members of the bridge are simulated by the 4-node shell63 element. The elastic modulus, Poisson ratio, and density of the selected steel were 206 GPa, 0.3, and 7850 kg/m^3, respectively. The contact of the connecting part of the members is to couple all the degrees of freedom of the node. Considering the vertical constraint of the suspender on the steel box girder, the suspender is simulated by the combine14 element. This element only considers the vertical constraints to simulate the tension provided by the cable to the bridge deck. According to the parameters such as the area, length, and elastic modulus of the cable, the stiffness required to simulate the cable by the combine14 element is 1.089e7 N/m. The following boundary conditions are applied to the model: constrain all degrees of freedom of the upper node of the suspender spring element; constrain the translation of S in longitudinal and transverse directions and the translation of N in longitudinal direction. For the substructure model of OSD, the area with a length of 6 m and width of 2.1 m (4 U-ribs) in the middle of the third lane span is selected, because of the highest probability of crack in the third lane. The segment model and substructure model of OSD are shown in Figure 4.

2.3. Local Damage Model. The stress due to fatigue of the orthotropic steel bridge deck is caused by the cyclic vehicle load directly acting on the deck. The local stress near the crack caused by residual stress and live load stress ranges is concentrated to a high level. The damage models of three typical fatigue cracks of OSD are shown in Figure 5. And, different damage types are described as follows.

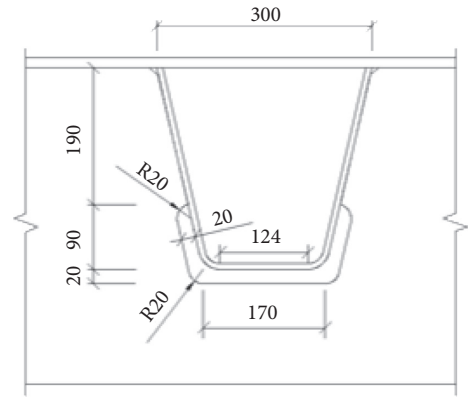

Figure 3: The arc-shaped notch.

The first damage type is a crack at the longitudinal rib-to-diaphragm welded joint.

The weld joint between longitudinal U-rib and diaphragm is one of the most complex geometric details in OSD. Under the local wheel load, the flexural deformation of longitudinal U-rib causes repeated out-of-plane deformation of the diaphragm. With the increase in deformation, the stress range will increase because of the welded defects and residual stress. In addition, the fatigue crack may be found on the rib wall or diaphragm at the longitudinal rib-to-diaphragm welded joint by the difference of stiffness between the longitudinal rib and the diaphragm and may expand along the weld to the deck and diaphragm. This connection is one of the most weld details prone to fatigue. In the substructure model, the crack was modeled at the connection between longitudinal rib and diaphragm:

Case 1: the crack appears at the connection between longitudinal U-rib 3R and diaphragm 2# and propagates about 200 mm along the weld.

Case 2: one-side weld between longitudinal U-rib and diaphragm is broken. And, the crack propagates forward and backward for 250 mm along the weld between the U-rib and the deck.

Case 3: one-side weld between longitudinal U-rib and diaphragm is broken, and the crack propagates 300 mm along the weld between the diaphragm and the deck.

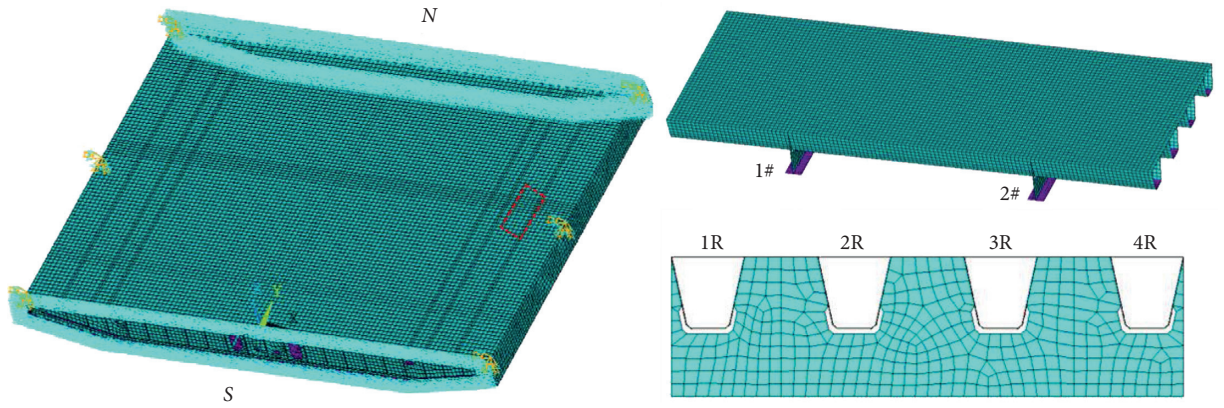

Figure 4: The steel box-girder segment model and the substructure model of OSD.

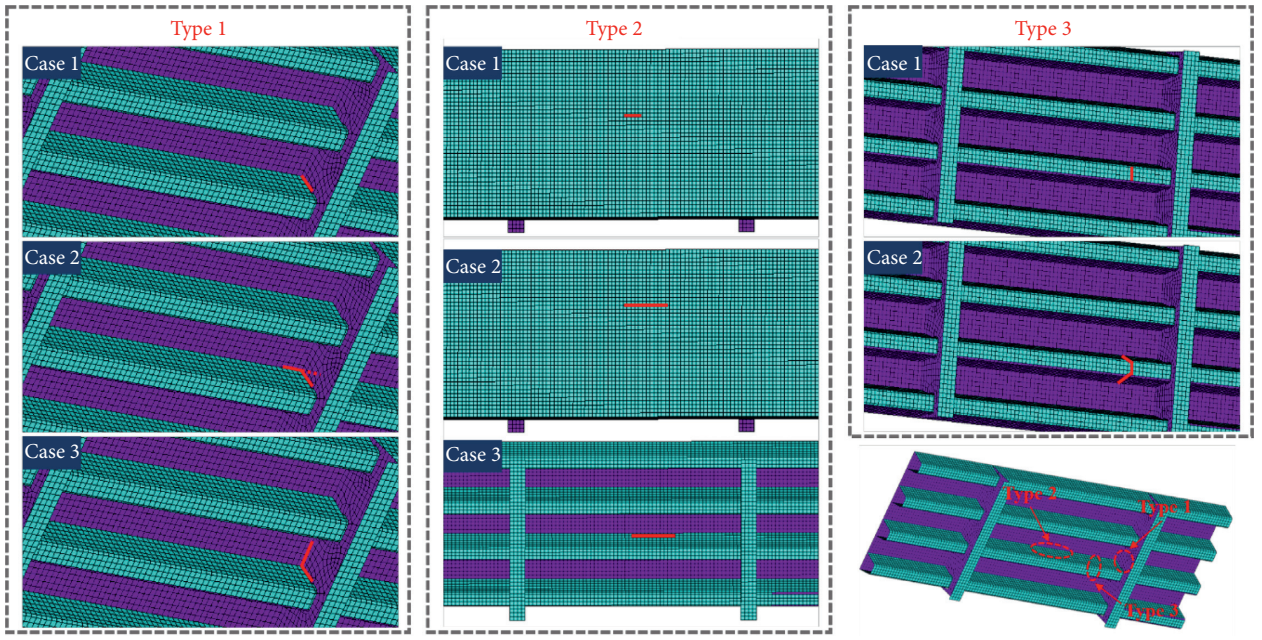

Figure 5: Typical crack distribution diagram.

The second damage type is a crack at the longitudinal rib-to-deck welded joint.

The longitudinal rib-to-deck welded joint is one of the most serious positions for fatigue in OSDs with direct local wheel loading. In addition, due to the difference of stiffness between the longitudinal rib and the deck, the stress ranges will be concentrated to a high level at the weld detail, which intensifies the initiation and propagation of fatigue cracks. Unfortunately, this type of fatigue crack monitoring is very difficult. Cracks can only be observed when they penetrate the deck and propagate along the weld, resulting in obvious damage to the bridge deck pavement. Moreover, the maintenance of fatigue cracks needs to interrupt the traffic. In the substructure model, the crack was modeled at the weld of the deck and the longitudinal U-rib 3R, which is located between the diaphragms:

Case 1: the crack appears on the weld root or weld toe of the deck at the longitudinal rib-to-deck welded joint and propagates about 200 mm along the weld

Case 2: the crack continues to propagate, resulting in a crack with a length of 850 mm at the deck between the two diaphragms

Case 3: the crack appears on the weld toe of the longitudinal rib at the longitudinal rib-to-deck welded joint and propagates into a crack with a length of 850 mm along the weld between the two diaphragms

The third damage type is a crack at the longitudinal rib splice joint.

The steel box girder is usually installed by single side overhead welding on-site. This welding process can only be carried out from the outside of the rib with incomplete penetration, resulting in cracks that are easy to initiate on the

weld root at the bottom of the longitudinal rib welded joint. Moreover, the welding of the longitudinal ribs splice joint accounts for about 40% of the total on-site welding of OSD, indicating that fatigue resistance of this weld has a very important influence on the safety of the bridge. In order to reduce the stress of the longitudinal U-rib splice joint, the splicing position is generally located at 1/4 of the space between the two diaphragms. Therefore, in the substructure model, the crack was modeled at 1/4 of the longitudinal U-rib 3R between the diaphragm:

Case 1: the crack appeared at the bottom of the weld at 1/4 of the longitudinal U-rib, with a length of 124 mm

Case 2: the crack continues to propagate, resulting in the complete failure of the butt weld of longitudinal U-rib 3R under the deck

3. Natural Vibration Frequency Analysis

The typical cracks described above were modeled at the corresponding positions of the orthotropic steel deck. For the global segment model and deck substructure model, a comparison of natural vibration frequencies and mode shapes has been studied with damaged and undamaged structures.

3.1. Global Vibration of the Steel Box-Girder Segment Model. Figure 6 shows the first 5 global natural vibration modes of the steel box-girder segment model with undamaged structure, and Table 1 describes the effects of different damage scenarios on global natural vibration frequency.

From the global vibration mode shapes of the steel box-girder segment model, it can be seen that the first 5 vibration modes include the vertical translational mode (the first vibration shape), bending mode (the second, fourth, and fifth vibration shapes), and torsional mode (the third vibration shape). Due to the different vibration mode shapes, the influence of different damage types on the natural vibration frequency of the global model is slightly different.

For the first vertical translational mode, the vertical vibration is only constrained by the vertical suspender. The vertical vibration is mainly related to the stiffness of the vertical suspender and the self-weight of the segment model, which are less affected by the different damages. According to the calculation results, the first natural frequency of the global model with damages is only 0.00099% lower than that of the healthy model. For the third torsional mode, the torsional vibration at the location of the damages is not dominant, so the influence of various types of damage on the torsional vibration frequency also is not obvious. The third natural frequency of the global model with damages is only 0.00165% lower than that of the complete model. For bending vibration mode, it can be clearly observed that the higher the bending vibration mode order, the greater the influence of damage on natural frequency. However, types and locations of the crack will affect the natural frequency of the structure. Since the crack locations are close to the amplitude of the fourth bending mode, most of the above damaged models have a greater decrease in amplitude in the fourth bending frequency than that in the second and fifth bending mode. Compared with the healthy model, the bending vibration frequency of the damaged model is reduced by 0.00249% (the second vibration mode shape), 0.01430% (the fourth vibration mode shape), and 0.01278% (the fifth vibration mode shape), respectively.

To summarize the above results for the different damages of the steel box girder, the cracks propagated on the deck have little effect on the vibration mode shapes and natural frequency of the global steel box girder. However, we also found that for similar types of vibration mode shapes, the higher the natural vibration frequency, the greater the impact of the damage. Therefore, we can guess whether the crack propagation will have a great impact on the local higher vibration mode and natural frequency of the steel box girder.

3.2. Local Vibration Model of OSD. The substructure model selected the area shown in Figure 4 for local vibration modes of OSDs. Modes 1–5 in Figure 7 show the local vibration modes of OSDs. In order to clearly observe the vibration of each part in the substructure model with no damage, a quarter of the grid of the model is treated perspectively. The higher modes mainly involved the local vibration of the deck, longitudinal U-rib, diaphragm, and the combined vibration of components, which should be a focus on the influence of damage on local modes.

Figure 8 shows local vibration modes with Type 1 damage of OSD. The changes of local natural frequency are given in Table 2. For this damage type, when the crack is in the initiation or only confined in the diaphragm (Case 1), the vibration mode shapes of the substructure with damage or no damage is consistent and the frequency changes slightly. The crack may propagate along the deck-longitudinal rib weld (Case 2) or the deck-diaphragm weld (Case 3), which will cause modal shapes of the substructure to change; for example, from Case 2 mode 1 and Case 3 mode 2 in Figure 8, the vibration mode shapes change obviously due to the existence of cracks and the frequency decreases greatly compared with the undamaged structure. In addition, from Case 3 mode 1 in Figure 8, the diaphragm near the damage has obvious out-of-plane deformation, which produces a new vibration mode shape. The reason may be that the damage weakens the restraint effect of the deck and U-rib on the diaphragm, which makes the vibration in the quiet area of the original mode shapes intense.

Figure 9 shows local vibration modes with Type 2 damage of OSD. The changes of local natural frequency are given in Table 3. For this damage type, the cracks may initiate at the weld root and rib-side weld toe of the longitudinal rib-to-deck weld in the span between two diaphragms. The above cracks with little propagation (Case 1) have no obvious impact on the local vibration mode shapes and natural frequencies. After that, the vibration mode shapes and natural frequencies will change greatly. For the crack propagation at the weld root (Case 2), the constrained boundary condition of the deck forms a free boundary near the damage, resulting in the amplitude of substructure

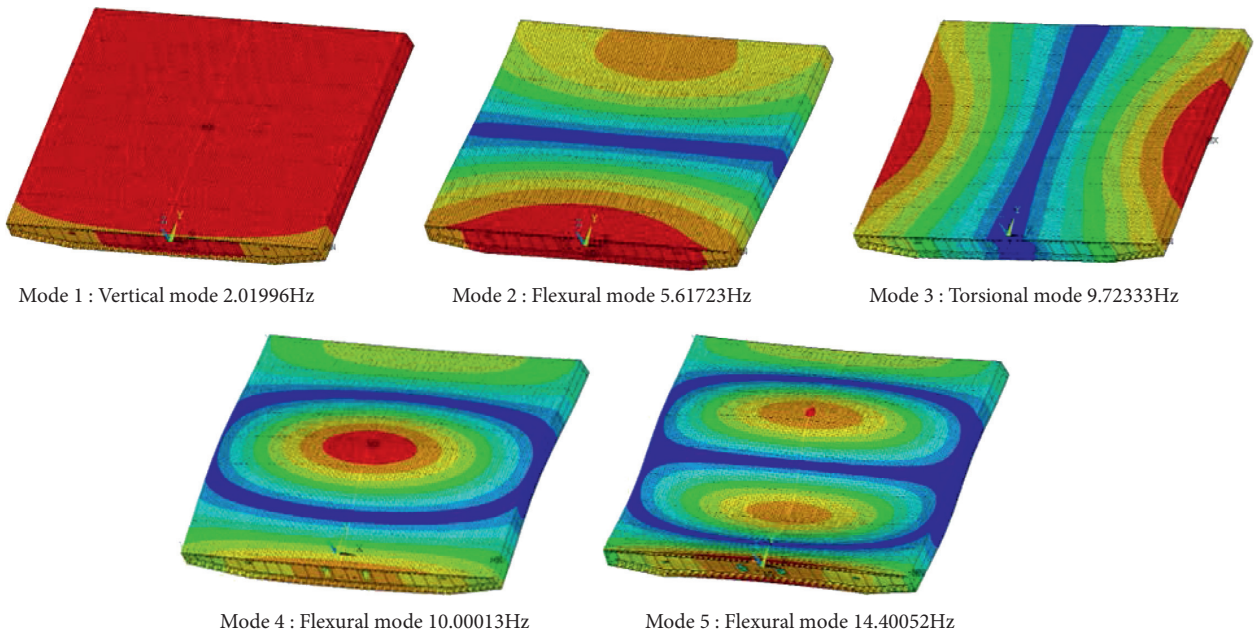

Figure 6: Global natural vibration mode shapes.

Table 1: Global natural vibration frequency.

Global mode	Healthy	Frequency (Hz)							
		Type 1			Type 2			Type 3	
		Case 1	Case 2	Case 3	Case 1	Case 2	Case 3	Case 1	Case 2
Mode 1	2.01996	2.01996	2.01995	2.01996	2.01996	2.01994	2.01996	2.01996	2.01996
Mode 2	5.61723	5.61723	5.61721	5.61723	5.61722	5.61717	5.61722	5.61723	5.61709
Mode 3	9.72333	9.72333	9.72317	9.72328	9.72332	9.72308	9.72333	9.72333	9.72330
Mode 4	10.00013	10.00012	9.99951	9.99998	10.00008	9.99870	10.00012	10.00011	9.99927
Mode 5	14.40052	14.40052	14.40014	14.40049	14.40049	14.39960	14.40052	14.40049	14.39868

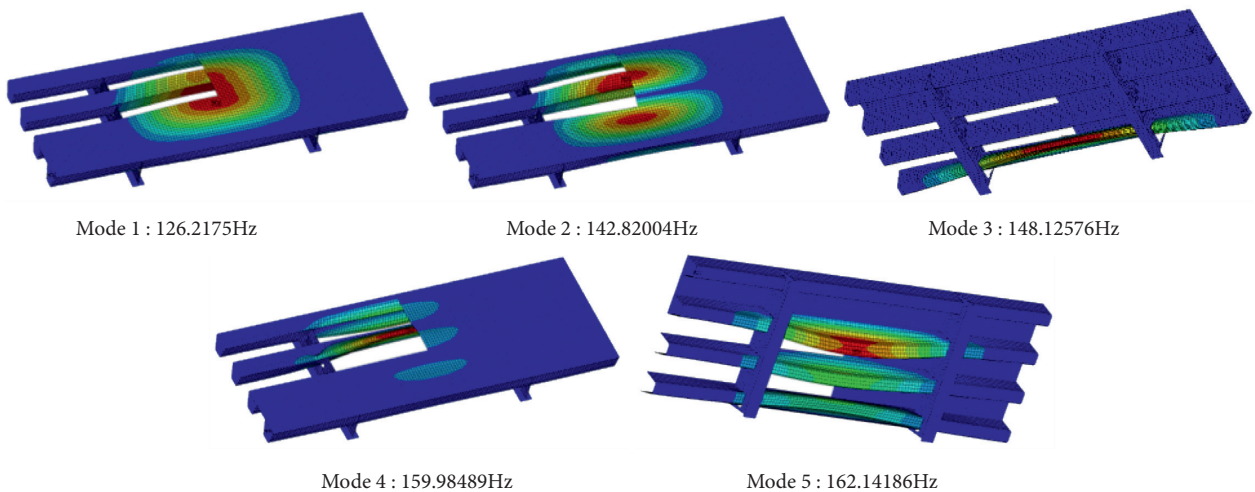

Figure 7: Local vibration mode shapes.

vibration shapes appearing at the damage, such as Case 2 mode 1 and mode 4 in Figure 9. The crack propagation at the rib-side weld toe (Case 3) weakens the constraint of the deck on the U-rib. The vibration mode shapes of the U-rib become a horizontal out-of-plane vibration. It is a new vibration mode shape, which greatly reduces the local natural frequency. It can be found that the crack of this damage type will greatly reduce the stiffness of the deck,

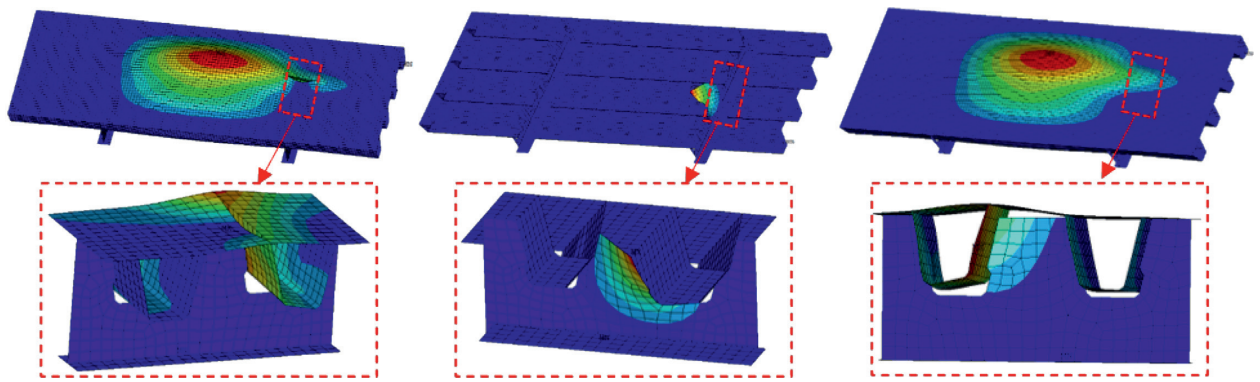

Figure 8: Local vibration mode shapes with Type 1 damage.

Table 2: Frequency of local vibration mode (Type 1 damage).

Local mode	Frequency (Hz)						
	Heathy	Case 1	Error (%)	Case 2	Error (%)	Case 3	Error (%)
1	126.21751	125.45765	−0.602	118.20422	−6.349	109.56704	−13.192
2	142.82004	142.54165	−0.195	140.18200	−1.847	117.87555	−17.466
3	148.12576	148.12061	−0.003	148.10308	−0.015	140.18688	−5.360
4	159.98489	158.16308	−1.139	158.07246	−1.195	148.10629	−7.425
5	162.14186	160.91106	−0.759	160.86859	−0.785	158.13833	−2.469

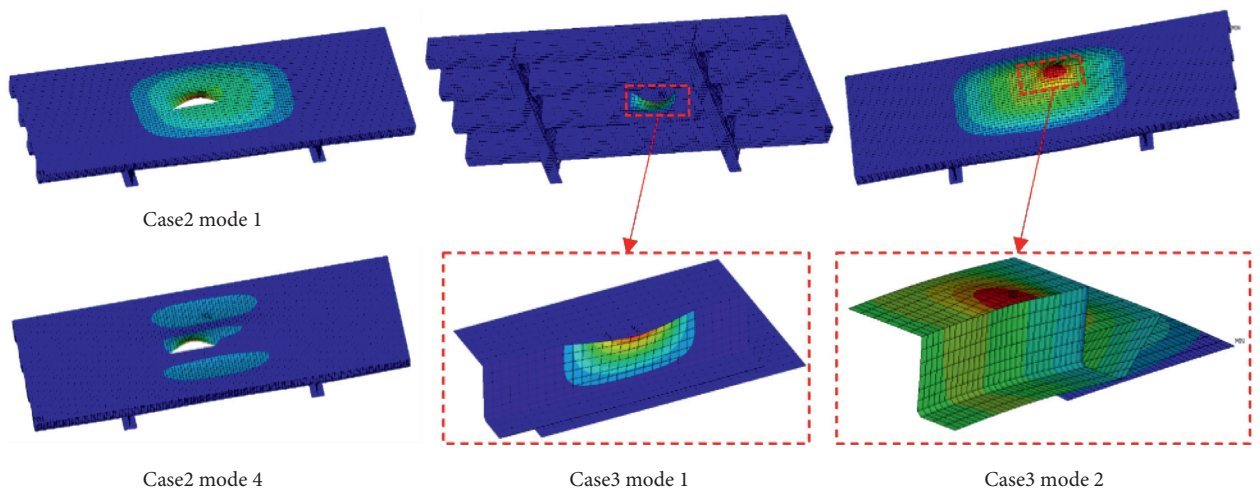

Figure 9: Local vibration mode shapes with Type 2 damage.

Table 3: Frequency of local vibration mode (Type 2 damage).

Local mode	Frequency (Hz)						
	Heathy	Case 1	Error (%)	Case 2	Error (%)	Case 3	Error (%)
1	126.21751	126.20012	−0.014	124.09384	−1.683	94.26651	−25.314
2	142.82004	142.72666	−0.065	141.71643	−0.773	123.3421	−13.638
3	148.12576	148.12542	−0.000	148.11960	−0.004	141.74663	−4.307
4	159.98489	159.98089	−0.0025	159.07485	−0.569	148.12468	−7.413
5	162.14186	162.11066	−0.019	161.87736	−0.163	159.93448	−1.361

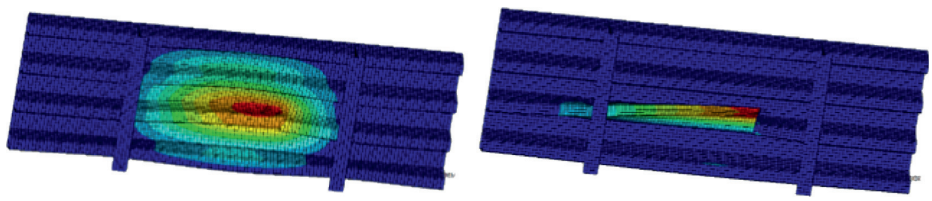

Case2 mode 1 Case2 mode 4

Figure 10: Local vibration mode shapes with Type 3 damage.

causing great harm to the bridge deck pavement, and even endanger traffic safety.

Figure 10 shows local vibration modes with Type 3 damage of OSD. The changes of local natural frequency are given in Table 4. For this damage type, crack initiation and propagation at the bottom of U-rib (Case 1) have no obvious impact on the local vibration mode and the frequency is almost unchanged. Then, the crack will propagate along the butt weld of the U-rib. The stiffness of longitudinal U-rib near the damage decreases greatly, resulting in the transfer of the vertical vibration mode in the middle of the span to the weld of 1/4 of the U-rib, such as Case 2 mode 1 in Figure 10. In addition, the existence of cracks weakens the constraints between U-ribs and also causes the horizontal distortion of U-ribs. Although this damage mode did not cause new vibration modes, it greatly weakens the stiffness of the longitudinal rib and reduces the natural frequency.

To summarize, for the local higher vibration modes of the substructure model, the initiation of fatigue cracks has no obvious effect on the vibration mode shapes and the natural frequencies. With the crack propagation, the local vibration modes and frequencies of the orthotropic steel bridge deck change greatly and even new vibration modes appear. Therefore, if it is possible to identify the local vibration mode of the structure, the fatigue crack type of the bridge deck can be predicted.

Table 4: Frequency of local vibration mode (Type 3 damage).

Local mode	Frequency (Hz)				
	Heathy	Case 1	Error (%)	Case 2	Error (%)
1	126.21751	126.07544	−0.113	119.06372	−5.668
2	142.82004	142.70092	−0.083	138.47059	−3.045
3	148.12576	148.12547	−0.000	147.37262	−0.508
4	159.98489	159.96930	−0.010	148.14346	−7.402
5	162.14186	162.10340	−0.024	160.46715	−1.033

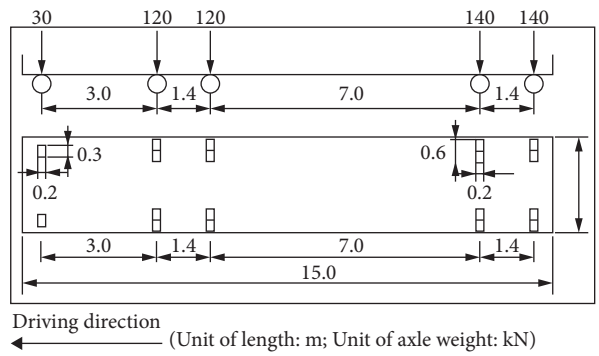

Figure 11: The vehicle traveling load.

4. Dynamic Response of the Traveling Vehicle

4.1. Traveling Vehicle Load. According to Chinese Code JTJ 021–89 [42], the vehicle traveling load is as shown in Figure 11. The vehicle was a five-axle vehicle with a total weight of 550 kN. The spacing and weight distribution of each axle are shown in Figure 11, respectively. Because the orthotropic steel deck is very sensitive to local load, the obvious local effect can be found only when the wheel load is close to the relevant details [43]. The spacing of the diaphragms (3 m) is significantly less than the spacing between the front and middle axles (3.7 m), and the axle weight of the front axle is small, far less than the middle and rear axles. Therefore, only the double axles of the rear axle (including two axles, the spacing is 1.4 m) were selected for vehicle load. Considering the influence of road roughness and other factors, an impact coefficient of 15% was added.

The loading procedure simulates the traveling of the vehicle on the deck. The calculation results of the wheel at 16 m in the middle of the bridge deck were selected to weaken the influence of boundary conditions. The moving route of the vehicle is shown in Figure 12. The vehicle load moved along the longitudinal direction of the bridge deck, with a uniform step of 0.2 m.

4.2. Change of the Dynamic Displacement Response. The variation of measured displacement is widely used to evaluate the loss of stiffness caused by damages to the bridge. Because different damage types have different contributions to the displacement response, we focused on the displacement of three parts: the welded joint between the longitudinal U-rib and the diaphragm, the midpoint of the longitudinal rib-to-deck welded joint between two diaphragms, and 1/4 of the longitudinal ribs splice joint, as shown in Figure 13.

Figure 14 shows the displacement with Type 1 damage change of three observation points under the traveling vehicle load (Z represents the distance between the center of double axle and the starting point). For Case 1, when the crack only existed at the connection between the diaphragm and the U-rib, the displacement of the three observation points was basically unchanged. However, when the crack

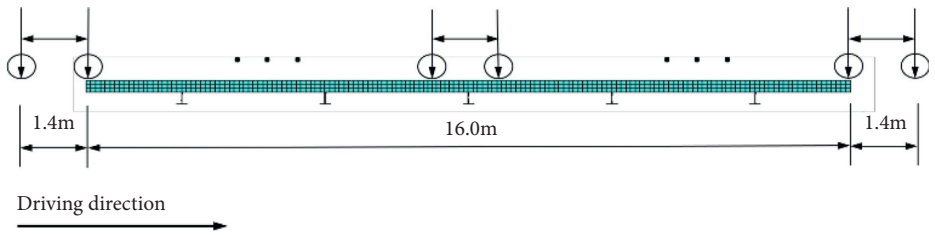

Figure 12: Distribution of the local wheel load.

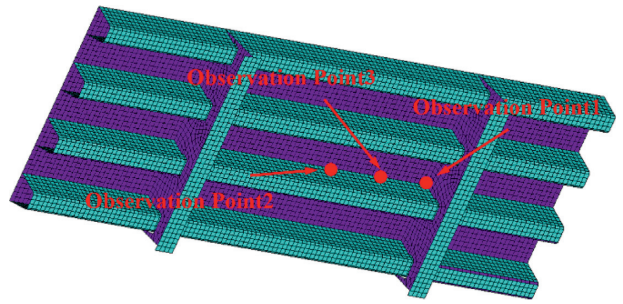

Figure 13: Location of the observation point.

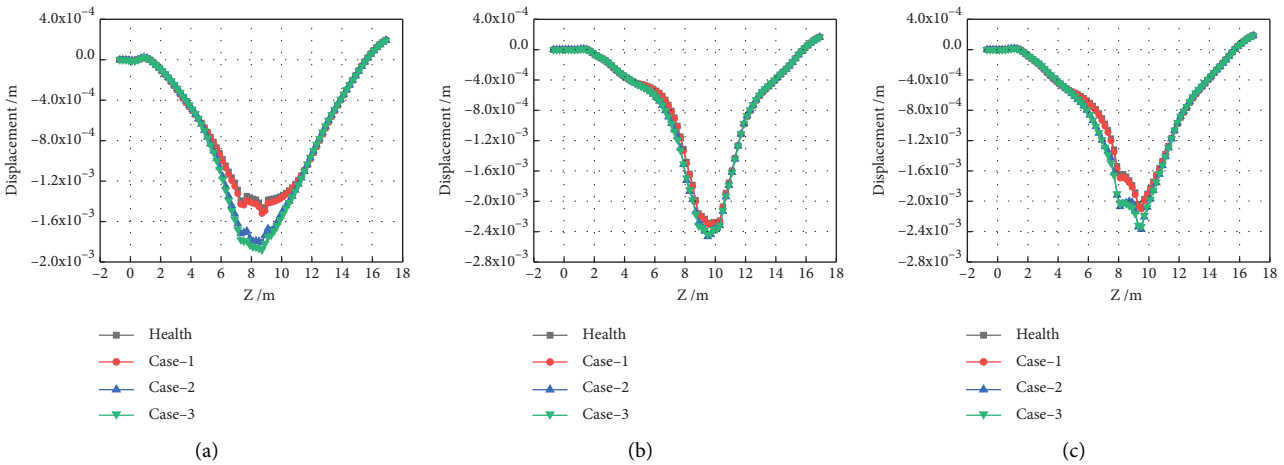

Figure 14: Displacement of observation point (Type 1 damage). (a) Observation point 1. (b) Observation point 2. (c) Observation point 3.

continued to propagate (such as Case 2 and Case 3), the displacement increased greatly. The displacement change recorded in Case 3 at observation point 1 was the largest, with an increase of 0.398 mm. The reason for this phenomenon may be that the crack of damage Type 1 reduced the constraint of the diaphragm and U-rib on the deck, resulting in a significant reduction in the stiffness near observation point 1. When the local wheel load travels above the deck, the corresponding displacement will also increase. Therefore, it is possible to identify crack damage Type 1 according to the displacement change recorded at observation point 1.

Figure 15 shows the displacement with Type 2 damage change of three observation points under the traveling vehicle load. For Case 1 and Case 2, with the crack propagation on the deck-side toe, the displacements of observation point 2 and observation point 3 changed slightly and the displacement of observation point 1 is basically unchanged. For Case 3, the crack propagation on the rib-side toe had obvious changes in the displacement recorded at observation point 2 with an increase of 0.370 mm. The reason for this phenomenon was that the crack invalidated the weld at the longitudinal rib-to-deck and the stiffness decreases greatly near observation point 2. When the local wheel load traveled above observation point 2, the displacement increased sharply. Therefore, it is possible to identify crack damage Type 2 according to the displacement changes recorded at observation point 2.

Figure 16 shows the displacement with Type 3 damage change of three observation points under the traveling vehicle load. For Case 1, the crack at the U-rib butt weld hardly affected the displacement of the three observation points. However, once the crack propagated along the butt weld (Case 2), the displacement will increase greatly. The

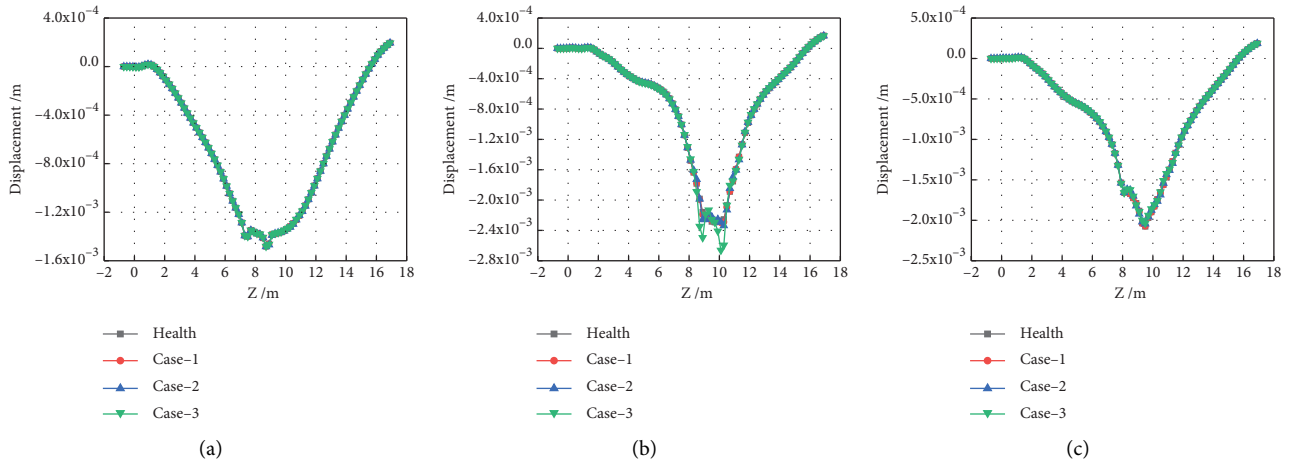

Figure 15: Displacement of observation point (Type 2 damage). (a) Observation point 1. (b) Observation point 2. (c) Observation point 3.

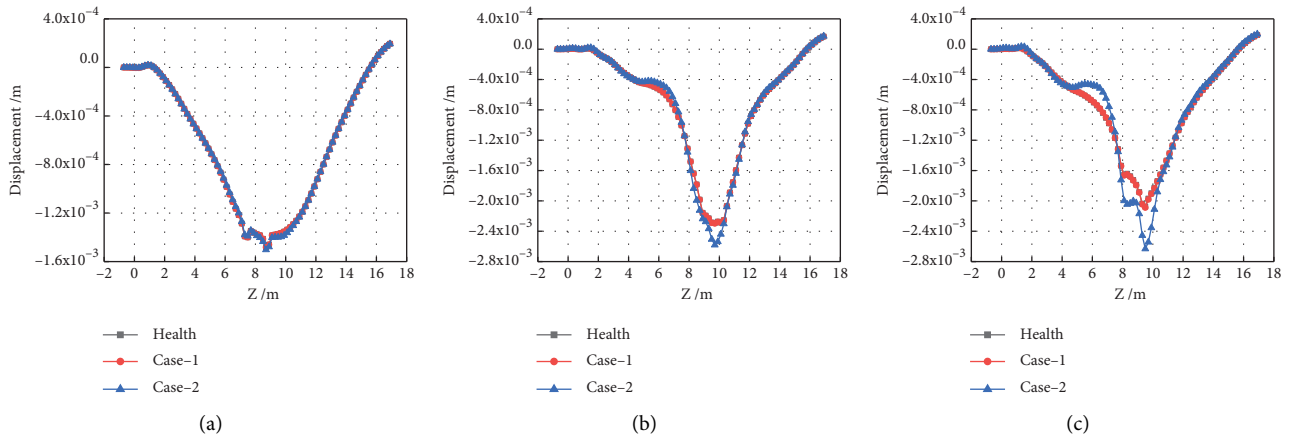

Figure 16: Displacement of the observation point (Type 3 damage). (a) Observation point 1. (b) Observation point 2. (c) Observation point 3.

displacement change recorded at observation point 3 was the largest, with an increase of 0.555 mm. The reason for this phenomenon was the sudden change of the stiffness at the weld due to the failure of the U-rib butt weld. When the center of the double axle just reached the weld failure position, the displacement increased obviously. Therefore, it is possible to identify crack damage Type 3 according to the displacement changes recorded at observation point 3.

5. Conclusion

In order to reveal the variation law of fatigue cracks on vibration frequency and deflection under vehicle load, global and local models of orthotropic steel decks with different types of damages caused by several cracks were established. The following conclusions could be obtained:

(1) Different damages slightly affect the vibration mode shapes and natural frequencies of the global steel box girder. For similar vibration mode shapes, the higher the frequency, the greater the impact of the damage.

(2) The cracks initiated on the local substructural mode of OSD have no obvious effect on the vibration mode shapes and natural frequencies. However, the damages caused by the propagated cracks will aggravate the vibration of the local model and even produce new vibration mode shapes.

(3) The different damages have different contributions to the dynamic displacement response of the bridge under vehicle load. Damage Type 1 will aggravate the displacement of the rib-to-diaphragm welded joint. Damage Types 2 and 3 will aggravate the displacement at the middle and 1/4 of the U-rib, respectively. Therefore, if the local mode of the orthotropic steel bridge deck and the displacement of key details under vehicle load can be obtained, it is possible to identify the damage type and predict the crack growth trend. This research can be used to provide

guiding significance for fatigue crack detection and maintenance.

Data Availability

The data used to support the findings of this study are included within the article.

Conflicts of Interest

The authors declare that they have no conflicts of interest.

Acknowledgments

This work was supported by the National Natural Science Foundation of China (grant number 51978550); Fundamental Research Funds for the Central Universities (grant number 2019-YB-024); Natural Science Foundation of Hubei Province (grant number 2016CFA020); and Key Research Plan of Ministry of Science and Technology (grant number 2018YFC0705601).

References

[1] D. Li, C. Zhang, and P. Lu, "Fatigue property and improvement of a rounded welding region between the diaphragm plate and closed rib of an orthotropic steel bridge deck," *Metals*, vol. 10, no. 2, p. 161, 2020.

[2] C. Cui, Y.-L. Xu, and Q.-H. Zhang, "Multiscale fatigue damage evolution in orthotropic steel deck of cable-stayed bridges," *Engineering Structures*, vol. 237, no. 3, Article ID 112144, 2021.

[3] Z. Fu, B. Ji, C. Zhang, and D. Li, "Experimental study on the fatigue performance of roof and U-rib welds of orthotropic steel bridge decks," *KSCE Journal of Civil Engineering*, vol. 22, no. 1, pp. 270–278, 2017.

[4] X. Jiang, Y. Yuan, C. Wu, and C. W. Luo, "Fatigue life assessment of orthotropic steel deck with UHPC pavement," *Journal of Engineering*, vol. 2017, Article ID 8413607, 2017.

[5] P. A. Tsakopoulos and J. W. Fisher, "Full-scale fatigue tests of steel orthotropic decks for the williamsburg bridge," *Journal of Bridge Engineering*, vol. 8, no. 5, pp. 323–333, 2003.

[6] S. Mustafa, H. Sekiya, M. Hayama, and C. Miki, "Effects of redecking from RC deck to orthotropic steel deck on seismic resistance of elevated girder bridges," *International Journal of Steel Structures*, vol. 20, no. 4, pp. 1393–1404, 2020.

[7] M. S. Pfeil, R. C. Battista, and A. J. R. Mergulhão, "Stress concentration in steel bridge orthotropic decks," *Journal of Constructional Steel Research*, vol. 61, no. 8, pp. 1172–1184, 2005.

[8] H.-T. Nguyen, Q.-T. Chu, and S.-E. Kim, "Fatigue analysis of a pre-fabricated orthotropic steel deck for light-weight vehicles," *Journal of Constructional Steel Research*, vol. 67, no. 4, pp. 647–655, 2011.

[9] N. Van den Berg, H. Xin, and M. Veljkovic, "Effects of residual stresses on fatigue crack propagation of an orthotropic steel bridge deck," *Materials & Design*, vol. 198, Article ID 109294, 2021.

[10] W. Nagy, E. Van Puymbroeck, K. Schotte, P. Van Bogaert, and H. De Backer, "Measuring residual stresses in orthotropic steel decks using the incremental hole-drilling technique," *Experimental Techniques*, vol. 41, no. 3, pp. 215–226, 2017.

[11] N. Lu, M. Noori, and Y. Liu, "Fatigue reliability assessment of welded steel bridge decks under stochastic truck loads via machine learning," *Journal of Bridge Engineering*, vol. 22, no. 1, Article ID 04016105, 2017.

[12] A. Duchaczek and Z. Mańko, "Influence of fatigue crack on strains state within assembly holes in a web of steel bridge girder," *International Journal of Civil Engineering*, vol. 15, no. 4, pp. 627–640, 2017.

[13] G.-N. Fanjiang, Q. Ye, O. N. Fernandez, and L. R. Taylor, "Fatigue analysis and design of steel orthotropic deck for bronx-whitestone bridge, New York city," *Transportation Research Record: Journal of the Transportation Research Board*, vol. 1892, no. 1, pp. 69–77, 2004.

[14] H. M. Salem and H. M. Helmy, "Numerical investigation of collapse of the Minnesota I-35W bridge," *Engineering Structures*, vol. 59, pp. 635–645, 2014.

[15] N. Ma and R. Wang, "Effects of impact loads on local dynamic behavior of orthotropic steel bridge decks," *International Journal of Steel Structures*, vol. 21, no. 1, pp. 132–141, 2020.

[16] B. Cheng, X. Ye, X. Cao, D. D. Mbako, and Y. Cao, "Experimental study on fatigue failure of rib-to-deck welded connections in orthotropic steel bridge decks," *International Journal of Fatigue*, vol. 103, pp. 157–167, 2017.

[17] Y. Liu, X. H. Xiao, N. W. Lu, and Y. Deng, "Fatigue reliability assessment of orthotropic bridge decks under stochastic truck loading," *Shock and Vibration*, vol. 2016, Article ID 4712593, 2016.

[18] F. Jiang, Z. Fu, B. Ji, and L. Wan, "Fatigue life evaluation of deck to U-rib welds in orthotropic steel deck integrating weldment size effects on welding residual stress," *Engineering Failure Analysis*, vol. 124, Article ID 105359, 2021.

[19] S. Kainuma, Y.-S. Jeong, M. Yang, and S. Inokuchi, "Welding residual stress in roots between deck plate and U-rib in orthotropic steel decks," *Measurement*, vol. 92, pp. 475–482, 2016.

[20] Y. Xiong, C. Li, Z. Chen, J. He, and H. Xin, "The evolution of residual stress in rib-diaphragm joints of orthotropic steel decks subjected to thermal cutting and welding," *Materials*, vol. 13, no. 17, p. 3804, 2020.

[21] S. Chen, Y. Huang, P. Gu, and J.-Y. Wang, "Experimental study on fatigue performance of UHPC-orthotropic steel composite deck," *Thin-Walled Structures*, vol. 142, pp. 1–18, 2019.

[22] R. Walter, J. F. Olesen, H. Stang, and T. Vejrum, "Analysis of an orthotropic deck stiffened with a cement-based overlay," *Journal of Bridge Engineering*, vol. 12, no. 3, pp. 350–363, 2007.

[23] M. Yang, B. Ji, Z. YuanZhou, and Z. Fu, "Fatigue behavior and strength evaluation of vertical stiffener welded joint in orthotropic steel decks," *Engineering Failure Analysis*, vol. 70, pp. 222–236, 2016.

[24] J.-H. Xu, G.-D. Zhou, and T.-Y. Zhu, "Fatigue reliability assessment for orthotropic steel bridge decks considering load sequence effects," *Frontiers in Materials*, vol. 8, Article ID 678855, 2021.

[25] M. Li, Y. Suzuki, K. Hashimoto, and K. Sugiura, "Experimental study on fatigue resistance of rib-to-deck joint in orthotropic steel bridge deck," *Journal of Bridge Engineering*, vol. 23, no. 2, Article ID 04017128, 2018.

[26] Y. Liu, F. Chen, D. Wang, and N. Lu, "Fatigue crack growth behavior of rib-to-deck double-sided welded joints of orthotropic steel decks," *Advances in Structural Engineering*, vol. 24, no. 3, pp. 556–569, 2020.

[27] Y. L. Zhang, Y. S. Li, and D. Y. Zhang, "Fatigue life estimation of rib-to-deck joints in orthotropic steel decks," *Advanced Materials Research*, vol. 163-167, pp. 410–416, 2010.

[28] S. Kainuma, M. Yang, Y.-S. Jeong, S. Inokuchi, A. Kawabata, and D. Uchida, "Experiment on fatigue behavior of rib-to-deck weld root in orthotropic steel decks," *Journal of Constructional Steel Research*, vol. 119, pp. 113–122, 2016.

[29] S. Kainuma, M. Yang, Y.-S. Jeong, S. Inokuchi, A. Kawabata, and D. Uchida, "Fatigue behavior investigation and stress analysis for rib-to-deck welded joints in orthotropic steel decks," *International Journal of Steel Structures*, vol. 18, no. 2, pp. 512–527, 2018.

[30] H.-B. Sim, C.-M. Uang, and C. Sikorsky, "Effects of fabrication procedures on fatigue resistance of welded joints in steel orthotropic decks," *Journal of Bridge Engineering*, vol. 14, no. 5, pp. 366–373, 2009.

[31] Q.-H. Zhang, C. Cui, Y.-Z. Bu, Y.-M. Liu, and H.-W. Ye, "Fatigue tests and fatigue assessment approaches for rib-to-diaphragm in steel orthotropic decks," *Journal of Constructional Steel Research*, vol. 114, pp. 110–118, 2015.

[32] J.-H. Choi and D.-H. Kim, "Stress characteristics and fatigue crack behaviour of the longitudinal rib-to-cross beam joints in an orthotropic steel deck," *Advances in Structural Engineering*, vol. 11, no. 2, pp. 189–198, 2008.

[33] B. Wang, "Fatigue assessment of the diaphragm-to-rib welded connection in orthotropic steel deck using effective notch stress approach," *Journal of Failure Analysis and Prevention*, vol. 15, no. 1, pp. 65–73, 2014.

[34] M Aygül, M Al-Emrani, and S Urushadze, "Modelling and fatigue life assessment of orthotropic bridge deck details using FEM," *International Journal of Fatigue*, vol. 40, pp. 129–142, 2012.

[35] K. Yokozeki and C. Miki, "Fatigue evaluation for longitudinal-to-transverse rib connection of orthotropic steel deck by using structural hot spot stress," *Welding in the World*, vol. 60, no. 1, pp. 83–92, 2015.

[36] Z. Fu, B. Ji, Z. Ye, and Y. Wang, "Fatigue evaluation of cable-stayed bridge steel deck based on predicted traffic flow growth," *KSCE Journal of Civil Engineering*, vol. 21, no. 4, pp. 1400–1409, 2016.

[37] J. Di, X. Z. Ruan, X. H. Zhou, J. Wang, and X. Peng, "Fatigue assessment of orthotropic steel bridge decks based on strain monitoring data," *Engineering Structures*, vol. 228, no. 1, p. 111437, 2020.

[38] M. Yang, S. Kainuma, and Y.-S. Jeong, "Structural behavior of orthotropic steel decks with artificial cracks in longitudinal ribs," *Journal of Constructional Steel Research*, vol. 141, pp. 132–144, 2018.

[39] Z. Xiao, K. Yamada, J. Inoue, and K. Yamaguchi, "Fatigue cracks in longitudinal ribs of steel orthotropic deck," *International Journal of Fatigue*, vol. 28, no. 4, pp. 409–416, 2006.

[40] Y. Nakasone, S. Yoshimoto, and T. A. Stolarski, *Engineering Analysis with ANSYS Software*, Elsevier Butterworth-Heinemann, 1st edition, 2006.

[41] Q. Wang, B. Ji, X. Chen, and Z. Ye, "Dynamic response analysis-based fatigue evaluation of rib-to-deck welds considering welding residual stress," *International Journal of Fatigue*, vol. 129, no. 9, Article ID 105249, 2019.

[42] Z. Y. Bao and Ministry of Communications of the People's Republic of China (Mcprc), *General Code for Design of Highway Bridges and Culverts*, JTJ 021-89, Beijing, 1989.

[43] Z. Zhu, T. Yuan, Z. Xiang, Y. Huang, Y. E. Zhou, and X. Shao, "Behavior and fatigue performance of details in an orthotropic steel bridge with UHPC-deck plate composite system under in-service traffic flows," *Journal of Bridge Engineering*, vol. 23, no. 3, Article ID 04017142, 2018.